CHINESE OPTICS LETTERS

Vol. 22, No. 2 | February 2024

On-chip stimulated Brillouin scattering [Invited]

Linfeng Yu (余林峰)†, Chukun Huang (黄楚坤)†, Ming Cheng (程 铭), Kang Wang (王 康), Haotian Shi (石浩天), Qiang Huang (黄 强), and Junqiang Sun (孙军强)*

Wuhan National Laboratory for Optoelectronics, Huazhong University of Science and Technology, Wuhan 430074, China

†These authors contributed equally to this work.

*Corresponding author: jqsun@mail.hust.edu.cn

Received August 26, 2023 | Accepted January 11, 2024 | Posted Online February 29, 2024

On-chip stimulated Brillouin scattering (SBS) has attracted extensive attention by introducing acousto-optic coupling interactions in all-optical signal processing systems. A series of chip-level applications such as Brillouin lasers, amplifiers, gyroscopes, filters, and nonreciprocal devices are realized based on Brillouin acousto-optic interaction. Here, we first introduce the fundamental principle of SBS in integrated photonics and a method for calculating Brillouin gain; then we illustrate the Brillouin effect on different material platforms with diverse applications. Finally, we make a concise conclusion and offer prospects on the future developments of on-chip SBS.

Keywords: stimulated Brillouin scattering; integrated photonics; silicon-on-insulator.
DOI: 10.3788/COL202422.020031

1. Introduction

Stimulated Brillouin scattering (SBS), a third-order optical nonlinearity, arises from a coherent interaction between guided optical waves and acoustic waves[1–3]. This inelastic scattering of light from acoustic phonons was first theoretically predicted by Brillouin in 1922[1]. However, the strict requirements of light source with strong intensity and narrow linewidth hindered the experimental observation of the SBS phenomenon in bulk media until 1964[4], soon after the invention of the laser. Moreover, the observation of SBS in optical fibers was first achieved in 1972[5]. Subsequently, numerous properties and applications based on SBS have been experimentally demonstrated in optical fibers and other bulk media over meter-scale propagation lengths[6–14]. This situation started to change when SBS was exploited in microstructure photonic crystal fibers (PCFs) in 2006[15], meaning that Brillouin interaction developed into a micrometer-scale structure. With the tight confinement of both optical waves and acoustic waves, Brillouin interaction could be significantly enhanced by the good overlap between optical and acoustic fields in microstructure. The first demonstration of on-chip SBS was realized on the chalcogenide soft glass integrated photonic platform in 2011[16], where the low stiffness and high refractive index of arsenic trisulfide (As_2S_3) satisfied the requirement of simultaneous confinement of both optical waves and acoustic waves. Subsequently, new theories were established to unlock the underlying mechanism of on-chip SBS[17–19], indicating that the radiation pressure on chip-scale waveguide boundaries was greatly magnified compared with bulk structure, which makes it possible to harness SBS in a chip-scale platform over centimeter-scale propagation lengths. Although silicon (Si) is considered to be a popular integrated photonic platform due to the compatibility with complementary metal-oxide-semiconductor (CMOS) technology, the confinement of acoustic waves in Si waveguides remains a key challenge to implement SBS for the leakage acoustic waves into silica (SiO_2) buried layer due to high stiffness. Therefore, there have been tremendous efforts and developments in the confinement of both optical waves and acoustic waves to control SBS interactions in Si waveguides as well as other novel waveguides and platforms over the past decade[3,16,20–31]. Additionally, a large amount of promising on-chip applications based on SBS have been demonstrated on different integrated photonic platforms[32–42].

In this paper, we review the various materials, structures, and methods to control and enhance on-chip SBS interactions in recent developments, as well as the progress in SBS-related properties and applications. This paper is divided into four parts and is arranged as follows. Section 1 gives a brief introduction about SBS, Section 2 introduces the basic principle and theory of SBS, Section 3 presents diverse devices and applications of on-chip SBS, and Section 4 is a concise outlook and conclusion of on-chip SBS.

2. Basic Principle and Theory of SBS

2.1. Basic overview

Brillouin scattering arises from the interaction between optical waves and acoustic waves. As shown in Fig. 1, the interaction of a pump wave and a Stokes wave optically induces an acoustic wave

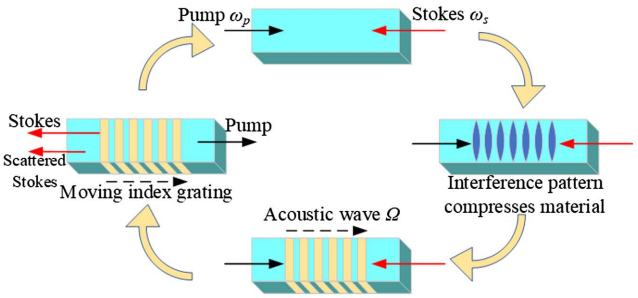

Fig. 1. Overview of SBS. Taking backward SBS, for example, the pump light ω_p and a counterpropagating Stokes light ω_s generate a beat pattern. This beat pattern generates a moving elastic wave Ω in the waveguide through electrostriction and radiation pressure, and the elastic wave perturbates the dielectric tensor of the material through the photoelastic effect, resulting in periodic refractive index changes in the waveguide. This periodic change in refractive index resembles a moving index grating, scattering the pump light to the Stokes light.

through electrostriction and radiation pressure, while the induced acoustic wave behaves as moving spatiotemporal gratings to further scatter the pump wave to the Stokes wave through photoelasticity and a moving boundary, which leads to a positive feedback loop between optical and acoustic fields[43]. From the quantum view, the process of Brillouin scattering is the coupling between photons and phonons, in which a pump photon is scattered to a redshifted Stokes or blueshifted anti-Stokes photon by creating or annihilating a phonon, as Fig. 2 depicts. Typically, the frequency of phonons in the SBS process is typically on the order of gigahertz, 5 orders of magnitude smaller than the frequency of photons.

Note that not all phonons could be coupled with photons in an SBS interaction; it requires both energy conservation and momentum conservation between photons and phonons, usually referred to as phase-matching requirements. Generally, SBS

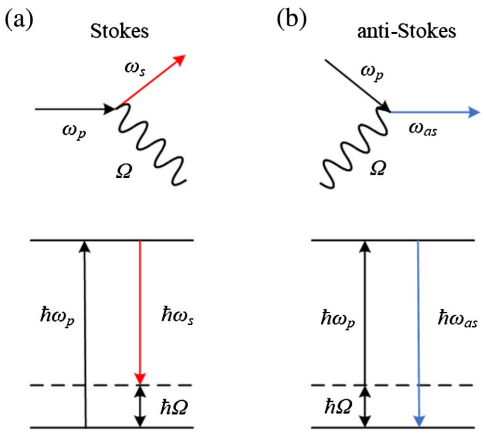

Fig. 2. Schematic of Brillouin acousto-optic interaction. (a) Stokes process; the pump photon is scattered into a redshifted photon and a phonon. (b) Anti-Stokes process; the pump photon absorbs a phonon and scatters into a blueshifted photon.

interaction in integrated waveguides can be divided into three types according to different dynamics: backward SBS (BSBS), intramodal forward SBS (FSBS), and intermodal FSBS. Figure 3 shows the simulated dynamics of these three different SBS types, including the distributions of the optical mode field, acoustic mode field, optical force field, and dispersion diagrams. The simulated waveguide cross-sectional dimensions are 1000 nm × 220 nm, which supports fundamental and first-order TE optical modes and multiple elastic wave modes.

2.1.1. Dynamics of BSBS

For BSBS interaction, the pump light and Stokes light are counterpropagating (the wave vectors are approximately $\boldsymbol{k}$ and $-\boldsymbol{k}$, respectively). Both lights are fundamental TE optical modes, with a frequency difference of Ω_m. The interaction between the pump light and Stokes light produces an electrostrictive force $\boldsymbol{if}^z(\boldsymbol{r}_\perp)$, mainly in the z direction, which is positively correlated with the photoelastic coefficient p_{12}. Meanwhile, the radiation pressure is generated perpendicular to the boundary of the waveguide. In BSBS interaction, the optical force is mainly contributed by electrostrictive force, leading to a traveling elastic wave propagating along the waveguide. As can be seen from the 3D view of the acoustic wave in Fig. 3(a), its main component is in the z direction.

By interacting with the traveling wave, energy is transferred from the pump light to the Stokes light, resulting in a single sideband Stokes gain. The visual diagram of the phase-matching requirements can be also found in Fig. 3(a). For optical waves with angular frequency ω_p and ω_s and wave vectors $\boldsymbol{k}_p$ and $\boldsymbol{k}_s$, the coupled acoustic wave should have an angular frequency of $\Omega_m = \omega_p - \omega_s$ and a wave vector of $\boldsymbol{q}_s = \boldsymbol{k}_p - \boldsymbol{k}_s \approx 2\boldsymbol{k}$. It is noted that the acoustic wave vectors required by the Stokes and anti-Stokes processes are reversed (for anti-Stokes process, $\Omega_m = \omega_{\text{as}} - \omega_p$ and $\boldsymbol{q}_{\text{as}} = -\boldsymbol{k}_p + \boldsymbol{k}_{\text{as}} \approx -2\boldsymbol{k}$); hence the two processes are decoupled in BSBS; that is, they cannot occur simultaneously. In the Stokes scattering process, a Stokes phonon is emitted, so the increased phonon occupancy increases the Stokes scattering rate, and this self-reinforcing mechanism eventually leads to the stimulated light scattering. In contrast, the anti-Stokes scattering process annihilates an anti-Stokes phonon, so there is no positive feedback loop, and thus it is impossible to produce the process of laser scattering. Therefore, only thermally excited phonons or externally injected phonons can sustain this process.

2.1.2. Dynamics of intramodal FSBS

For intramodal FSBS interaction, the pump light and Stokes light are co-propagating (the wave vectors are both approximately $\boldsymbol{k}$), and both lights are fundamental TE optical modes. The interaction between the pump light and Stokes light produces an electrostrictive force $\boldsymbol{f}^x(\boldsymbol{r}_\perp)$, mainly in the x direction, which is positively correlated with the photoelastic coefficient p_{11}. Meanwhile, the radiation pressure is generated perpendicular to the boundary of the waveguide. In intramodal

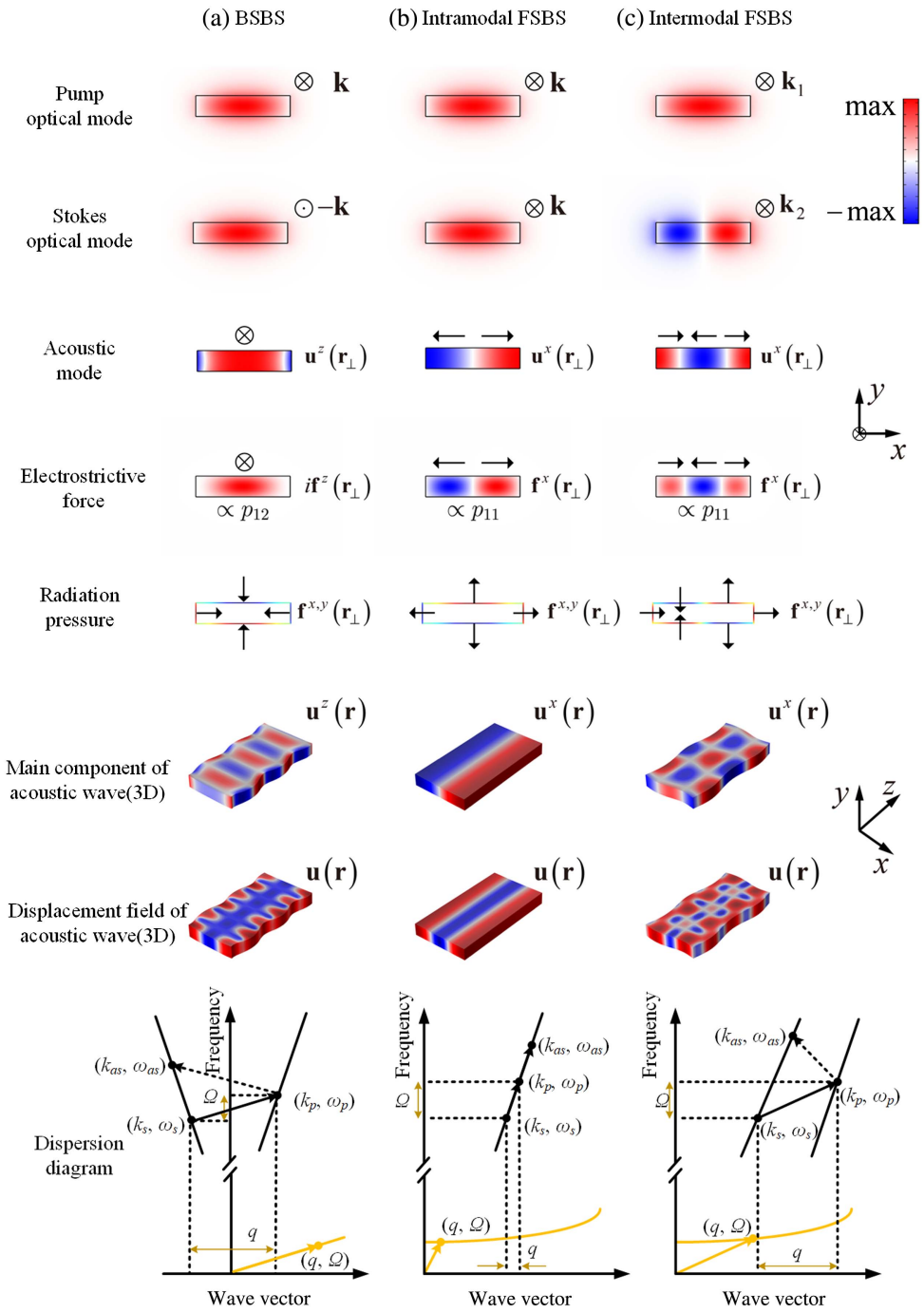

Fig. 3. Dynamics of three different SBS types in integrated waveguides. (a) BSBS; (b) intramodal FSBS; (c) intermodal FSBS.

FSBS, both the electrostrictive force and the radiation pressure contribute to the optical force and have the same symmetry as the acoustic wave, leading to a transverse standing-wave-like mode ("breath mode"); that is, the wave vector $\boldsymbol{q}$ is nearly 0. As can be seen from the 3D view of the acoustic wave in Fig. 3(b), its main component is in the x direction.

The dynamics of intramodal FSBS are significantly different from those of BSBS, resulting in the coupling of multiple sidebands, which scatter light to many different frequency components. The energy transfer process of the multiple sidebands is due to the coupling of Stokes and anti-Stokes processes to the same acoustic mode. As shown in Fig. 3(b), the Stokes, pump, and anti-Stokes optical states are on the collinear light dispersion curve in the low dispersion state. The same acoustic mode is simultaneously phase-matched to the Stokes and anti-Stokes scattering processes ($\boldsymbol{q}_s = \boldsymbol{q}_{\rm as} = \boldsymbol{k}_p - \boldsymbol{k}_s$, $\Omega_m = \omega_p - \omega_s = \omega_{\rm as} - \omega_p$), so that the Stokes and anti-Stokes processes are inherently coupled together in intramodal FSBS[44]. Compared with the two-field coupling and exponential amplification of BSBS, intramodal FSBS is a kind of

traveling-wave phase modulation, which produces cascaded energy transfer to continuous modulation levels[45]. Because of this mechanism, the generation and annihilation of phonons in intramodal FSBS are essentially balanced, leading to a spatially constant amplitude of the acoustic field. Therefore, the stimulated phonon gain cannot be obtained. As a result, intramodal FSBS cannot generate laser scattering from thermal noise like BSBS, so it is not suitable for building self-excited oscillating Brillouin lasers directly[44].

2.1.3. Dynamics of intermodal FSBS

For intermodal FSBS interaction, the pump light and Stokes light are co-propagating (the wave vectors are $\boldsymbol{k}_1$ and $\boldsymbol{k}_2$, respectively), but the pump and Stokes light are of different optical mode families (here assuming that the pump light is fundamental TE mode and Stokes light is first-order TE mode). Similar to intramodal FSBS, the electrostrictive force is also mainly in the x direction. The excited acoustic wave (Lamb-like mode) in intermodal FSBS has both transverse and longitudinal components, as can be seen from the 3D view of the acoustic wave in Fig. 3(c).

According to the dispersion diagram in Fig. 3(c), intermodal FSBS occurs in two distinct optical dispersion branches in the forward direction, and the Stokes scattering process causes light to scatter from the fundamental optical mode to the first-order optical mode. The coupled acoustic wave should have an angular frequency of $\Omega_m = \omega_p - \omega_s$ and a wave vector of $\boldsymbol{q}_s = \boldsymbol{k}_p - \boldsymbol{k}_s$. Because of the waveguide dispersion, the two optical modes may have different phase velocities, and the acoustic wave vector can be changed by tailoring the structure of the waveguide. Since the optical coupling occurs in different optical dispersion curves (for anti-Stokes process, $\Omega_m = \omega_{\rm as} - \omega_p$ and $\boldsymbol{q}_{\rm as} = -\boldsymbol{k}_p + \boldsymbol{k}_{\rm as}$), the phonons involved in the Stokes and anti-Stokes processes have different wave vectors with opposite directions, and the symmetry of Stokes and anti-Stokes processes is broken again. Thus, the Stokes and anti-Stokes processes are decoupled in intermodal FSBS, and a single sideband energy transfer process similar to BSBS is restored, which provides the necessary conditions for stimulated phonon gain and Brillouin lasers[28].

2.2. SBS coupled-mode equations

While the Brillouin interactions were implemented in waveguide systems below optical wavelength scale, new mechanisms were discovered and theoretically analyzed that were not observed in the bulk SBS process[17–19]. Apart from the modified refractive index distribution induced by electrostriction in bulk materials, the induced acoustic motion also modifies the refractive index distribution near the waveguide boundary with small cross sections because fractional material is replaced by the surrounding material or air. Another new mechanism is that strong radiation pressure, comparable with electrostriction, is induced by the interaction of optical waves on the high refractive index contrast boundary, which results in the feasibility of forward Brillouin scattering on the integrated photonic platform.

The coupled-mode equations of Brillouin interactions have been extensively derived through classical methods and quantum Hamiltonian methods[17–19,46–53]. The consequence of coupled-mode equations derived either by classical or quantum methods is consistent. The SBS process is a three-wave interaction among the pump, Stokes, and acoustic wave, governed by the following coupled-mode equations in waveguides[50]:

$$\partial_z a_p + \frac{1}{v_p}\partial_t a_p + \frac{\alpha_p}{2} a_p = -i\frac{\omega_p}{\mathcal{P}_p} g a_s b, \tag{1}$$

$$\partial_z a_s + \frac{1}{v_s}\partial_t a_s + \frac{\alpha_s}{2} a_s = -i\frac{\omega_s}{\mathcal{P}_s} g^* a_p b^*, \tag{2}$$

$$\partial_z b + \frac{1}{v_m}\partial_t b + \left(i\delta_m + \frac{\alpha_m}{2}\right) b = -i\frac{\Omega_m}{\mathcal{P}_m} g^* a_p a_s^*, \tag{3}$$

where a_p, a_s, and b are the slowly varying amplitude envelopes and $\mathcal{P}_{p,s,m}$ represent the normalized powers of pump, Stokes, and acoustic waves, respectively. In addition, $v_{p,s,m}$ and $\alpha_{p,s,m}$ represent the group velocities and power attenuation coefficient ($[{\rm m}^{-1}]$) of pump, Stokes, and acoustic waves, respectively. $\delta_m = \boldsymbol{q} - (\boldsymbol{k}_p - \boldsymbol{k}_s)$ is the wave vector mismatch between optical and acoustic waves, and $g = \int \boldsymbol{f} \cdot \boldsymbol{u}^* \, {\rm d}^2 r$ is Brillouin coupling constant that represents the strength of optoacoustic interaction between the total optical force $\boldsymbol{f}$ and acoustic displacement $\boldsymbol{u}$.

For Brillouin interaction within the nanoscale structure, the total optical force is contributed by electrostrictive body force $\boldsymbol{f}^{\rm ES,body}$, electrostrictive boundary force $\boldsymbol{f}^{\rm ES,boundary}$ (generally can be ignored), and radiation pressure $\boldsymbol{f}^{\rm RP}$. Electrostriction is the elastic deformation of dielectric materials because of the presence of an electric field. The electrostrictive body force is then generated where the optical intensity gradient exists. This body force with vector components can be written as[46]

$$f_i^{\rm ES,\,body} = -\partial_j \sigma_{ij}, \tag{4}$$

where σ_{ij} is the electrostrictive tensor element and can be expressed as

$$\sigma_{ij} = -\frac{1}{4}\varepsilon_0 n^4 p_{ijkl}(E_{pk}E_{sl}^* + E_{pl}E_{sk}^*), \tag{5}$$

where ε_0 denotes the vacuum permittivity, n is the refractive index, p_{ijkl} is the photoelastic tensor, and $E_{p(s)}$ represent the electric fields of the pump and Stokes waves, respectively. In addition, there will be an additional electrostrictive boundary force at the material interface because of the difference in electrostrictive stress, which is given by

$$f_i^{\rm ES,\,boundary} = (\sigma_{1ij} - \sigma_{2ij})\hat{n}_j. \tag{6}$$

Here, $\hat{n}_j$ is the component of the normal vector pointed from material 1 to material 2.

The radiation pressure is induced by a Maxwell stress tensor at the discontinuous boundary, which is given by

$$f_i^{\mathrm{RP}} = (T_{2ij} - T_{1ij})\hat{n}_j, \tag{7}$$

where T_{ij} is the Maxwell tensor element and can be expressed as

$$T_{ij} = \varepsilon_0 \varepsilon \left(E_i E_j - \frac{1}{2}\delta_{ij} E^2 \right). \tag{8}$$

Typically, in the steady-state ($\partial_t \to 0$) and large acoustic damping ($\alpha_m \gg \alpha_{p,s}$) regime, the slowly varying envelope of the acoustic wave can be adiabatically simplified to $b = -i(\Omega_m/\mathcal{P}_m) g^* a_p a_s^* / (i\delta_m + \alpha_m/2)$. Thus, we can retrieve the coupled equations between pump and Stokes powers ($P_{p,s} = |a_{p,s}|^2 \mathcal{P}_{p,s}$) along the waveguide length, governed by

$$\partial_z P_p = -G_B P_p P_s - \alpha_p P_p, \tag{9}$$

$$\partial_z P_s = G_B P_p P_s - \alpha_s P_s, \tag{10}$$

where G_B is the well-known Brillouin gain with a unit of [$\mathrm{W^{-1}\,m^{-1}}$], expressed as

$$\begin{aligned} G_B(\Omega) &= \frac{2\omega\Omega_m |g|^2}{\mathcal{P}_p \mathcal{P}_s \mathcal{P}_m} \frac{\alpha_m/2}{\delta_m^2 + (\alpha_m/2)^2} \\ &= \frac{4\omega Q_m |g|^2}{\mathcal{P}_p \mathcal{P}_s \mathcal{E}_m} \frac{(\Gamma_m/2)^2}{(\Omega - \Omega_m)^2 + (\Gamma_m/2)^2}, \end{aligned} \tag{11}$$

where the response of Brillouin gain coefficient G_B is the Lorentzian profile related to the acoustic mode with the approximation of $\omega_p \approx \omega_s = \omega$. Here, $Q_m = \Omega_m/\Gamma_m$ is the acoustic quality factor with the acoustic damping rate $\Gamma_m = \nu_m \alpha_m$, $\mathcal{E}_m = \mathcal{P}_m/\nu_m$ is the normalized acoustic energy density per unit length, and $\Delta_m = \Omega - \Omega_m = \nu_m \delta_m$ is the frequency mismatch.

SBS cavities, also referred to as optomechanical cavities, can be regarded as Brillouin-active waveguides with a round-trip length L. Then, by applying mean-field approximation, the term of ∂_z can be eliminated. Hence, the coupled-mode equations for cavities are governed by[50]

$$\partial_t a_p + (i\Delta_p + \kappa_p/2) a_p = -i g_0 a_s b + \sqrt{\kappa_{\mathrm{cp}}} s_p, \tag{12}$$

$$\partial_t a_s + (i\Delta_s + \kappa_s/2) a_s = -i g_0^* a_p b^* + \sqrt{\kappa_{\mathrm{cs}}} s_s, \tag{13}$$

$$\partial_t b + (i\Delta_m + \Gamma_m/2) a_s = -i g_0^* a_p a_s^* + \sqrt{\kappa_{\mathrm{cm}}} s_m, \tag{14}$$

where a_p, a_s, and b are the normalized slowly varying envelopes such that $|a_p|^2$, $|a_s|^2$, and $|b|^2$ represent the average number of cavity photons or phonons of pump, Stokes, and acoustic waves, respectively. In addition, $\kappa_{p,s}$ and $\Delta_{p,s} = \omega_{p,s} - \omega_{p0,s0}$ are the optical damping rate and frequency detuning between input fields $\omega_{p,s}$ and cavity modes $\omega_{p0,s0}$ of pump and Stokes waves, respectively. The input field envelopes $s_{p,s,m}$ are coupled to cavities with a rate of $\kappa_{\mathrm{cp,cs,cm}}$. The single-photon optomechanical coupling rate g_0 ([rad/s]) represents the frequency shift of the optical mode induced by the single-phonon acoustic motion, derived from the perturbation theory and given by

$$g_0 = x_{\mathrm{zpf}} \frac{\partial \omega}{\partial x}, \tag{15}$$

where $x_{\mathrm{zpf}} = \sqrt{\hbar/(2 m_{\mathrm{eff}} \Omega)}$ is the zero-point fluctuation of the acoustic modes with the effective mass $m_{\mathrm{eff}} = \int \rho |\boldsymbol{u}|^2 / \max |\boldsymbol{u}|^2 \mathrm{d}V$.

In general, the Brillouin gain G_B is the key metric for Brillouin-active waveguides, while the optomechanical coupling rate g_0 is the key metric for optomechanical cavities or Brillouin cavities. Moreover, these parameters can be accurately computed by using commercial numerical solvers[17–19,46,48,50,54] with full-vector methods.

3. Devices and Applications of On-Chip SBS

3.1 SBS devices with different materials and structures

As mentioned above, the Brillouin gain G_B, pump power, and interaction length are all the significant metrics for SBS interaction. To achieve efficient Brillouin interactions in the integrated guided-wave systems, the material properties and waveguide dimensions as well as type of SBS process need to be taken into consideration. The main strategy is to optimize the Brillouin gain G_B, which depends on the photoelastic coefficients of materials and the overlap between optical forces and acoustic displacements. Meanwhile, the acoustic waves could be optically excited by electrostriction and radiation pressure[25–28,53], electrically excited by external piezoelectricity[31,55–57], or thermally excited by thermoelasticity associated with the thermal phonons[26]. To obtain good overlap between optical forces and acoustic displacements, simultaneous confinement of optical and acoustic fields is necessary in a waveguide. Although the optical fields are easy to confine through total internal reflection with high refractive index contrast, the acoustic fields may not be so easy to confine on-chip.

The acoustic impedance of a medium is $Z_m = \rho v_\varphi$ with the acoustic phase velocity v_φ and mass density ρ, which plays a significant role for acoustic fields analogous to the refractive index for optical fields. There are three common strategies to confine acoustic fields. First, select an appropriate waveguide material with low stiffness to have the lowest acoustic velocity in the surrounding materials[16,34]. Second, confine the acoustic fields through acoustic impedance mismatch. This causes a large acoustic impedance mismatch between solid materials and air so that the acoustic fields are confined to solid materials. For instance, the suspended waveguides[26,51,58–60] and partial suspended waveguides supported by a thin pedestal[27,54,61–64] can effectively confine acoustic fields to waveguides. Third, confine the acoustic fields through phononic bandgaps[3,65–69]. Similar to photonic crystals, the phononic crystals shield and

reflect the phonons within the bandgap so that we can implement phononic crystals on either side of the waveguides to confine the acoustic fields to waveguides.

Apart from photoelastic coefficients, another key material property that needs to be taken into consideration is the optical propagation loss[53]. Although the SBS interaction length on an integrated photonic platform is centimeter-scale (largely shorter than in meter-scale optical fibers), it is still fairly long compared with optical wavelength so that the optical propagation loss should be considered in the SBS process. In addition, nonlinear optical losses, including two-photon absorption (TPA) and TPA-induced free carrier absorption (FCA), are detrimental to optical power as well as SBS interaction in semiconductor materials, especially in the high optical power regime[3,49]. Consequently, the ability to handle high optical powers is limited by the nonlinear optical losses, and the optical propagation loss is mostly dependent on linear optical loss in the low pump power regime. Thus, to realize effective Brillouin interaction, Brillouin-active materials should have the properties of large photoelastic coefficients and low optical propagation loss. Figure 4 presents the typical on-chip SBS devices with different materials and structures.

The first experimental demonstration of on-chip SBS was implemented in an As_2S_3 rib waveguide on an integrated photonic platform[16]. As_2S_3, one of chalcogenide glasses, is a kind of perfect material for the SBS process because it can simultaneously satisfy the strict requirements of having a large photoelastic coefficient, high refractive index, and low stiffness (Table 1 shows the commonly used material platforms and the corresponding properties for on-chip SBS[2,29,63,64,70–75]). Combined with these material properties, optical and acoustic fields are confined to As_2S_3 waveguide and Brillouin gain G_B is about a hundredfold times that of silica optical fiber[16]. Additionally, low optical loss (typically 0.4–0.5 dB/cm) and good power handling (more than 500 mW) enable the long SBS interaction length (~22 cm). Therefore, large on/off gains (52 dB) and net gains (40 dB) are able to be achieved in an As_2S_3 waveguide[76,77]. Backward Brillouin lasing was thus stimulated utilizing a spiral ring resonator composed of a 5.8-cm long As_2S_3 waveguide[25]. The on-chip threshold is about 50 mW with a slope efficiency of 4%.

With optical fiber made of silica, it is easy to observe strong spontaneous Brillouin scattering due to the extreme loss and kilometer-scale interaction length. However, it is hard to implement the Brillouin process in silica waveguides on an integrated photonic platform because optical fields may not be effectively confined to silica waveguides on an SI substrate due to the low refractive index of silica. Fortunately, we can still exploit the extreme intrinsic loss and large photoelastic coefficients of SiO_2 (Table 1) through a silica whispering-gallery resonator (WGR). The unload quality (Q) factor of silica WGR can easily reach 10^8[27,78]. Therefore, its internal energy density is very high, which is quite beneficial for the excitation of Brillouin lasing. SBS in silica WGRs was first reported in the microsphere[20]. This 100-μm diameter microsphere has a Q factor of 3×10^8, and the backward Brillouin lasing will be excited when the pump power exceeds 26 μW with a slope efficiency over 90%. Subsequently, forward Brillouin lasing was also demonstrated in the silica microsphere[22] and Brillouin frequency shifts ranging from 58 MHz to 1.408 GHz were achieved. However, the SBS for on-chip WGR was realized only after the ultrahigh Q wedge microdisk manufacturing process was proposed[23]. The diameter of the microdisk is about 6 mm to satisfy the free spectrum range (FSR) equal to the Brillouin frequency (~11 GHz). This WGR Brillouin device can also be integrated monolithically with other functional devices through a silicon nitride (Si_3N_4) coupling waveguide[24].

Silicon-on-insulator (SOI) is the most popular integrated photonic platform because it is compatible with CMOS manufacturing technology. Compared with As_2S_3 and silica, Si has small photoelastic coefficients, high stiffness, and a large refractive index (Table 1). The large refractive index of Si enables the design of small optical mode area waveguide, which enhances the optical nonlinearity, including Brillouin interaction[61]. However, the high stiffness with large acoustic velocity results in poor acoustic confinement and acoustic mode leakage on SOI platforms. Therefore, great efforts have been made to confine acoustic fields in Si waveguides, such as suspended Si or hybrid Si-Si_3N_4 structures[26,28,58,79], Si waveguides with nanoscale silica pillar support[27,61,62,80], and Si waveguides with phononic crystals[3,65,67–69,81]. With these special designs, the optical fields and acoustic fields could be simultaneously confined to small cross-sectional Si waveguides so that Brillouin interaction is greatly enhanced. The dominant SBS processes are intramodal and intermodal FSBS in Si waveguides rather than BSBS because $p_{11} \gg p_{12}$ in Si, which means that the electrostriction force of FSBS is greater than that of BSBS (Fig. 3). Nevertheless, the power handling and SBS interaction efficiency are limited by the large TPA and FCA coefficients in Si[3,49]. Thus, there is a trade-off between optical loss and Brillouin gain in the design of Si Brillouin devices. The first experimental demonstration of SBS on SOI was implemented in a 4.9-mm long suspended hybrid Si-Si_3N_4 waveguide[26]. Although the on/off gain was 0.374 dB, no positive net gain was obtained (−1.935 dB) due to the relatively high linear loss. With the further improvement of the fabrication process and structure, positive net gains have been reported[28,42,59,79]. After that, the introduction of phononic crystals can provide selectivity to the excited acoustic modes through the phononic bandgap effect[3], avoiding the detrimental influence of the undesired acoustic modes. By utilizing ring-resonator-composed Si waveguides, large forward Brillouin amplifying[42] and Brillouin lasing[53] with a slope efficiency of 3% were then achieved.

Recently, Brillouin interactions have been implemented not only in suspended Si_3N_4 waveguides for the forward SBS process on CMOS-compatible platforms but also in leaky Si_3N_4 waveguides without acoustic confinement for the backward SBS process[29,70,82]. Although it was found that the photoelastic coefficient of Si_3N_4 is much smaller compared with other Brillouin-active materials (Table 1), the relative low Brillouin gain of Si_3N_4 is compensated for by resonant enhancement within an ultralow loss optical cavity. Germanium (Ge) is

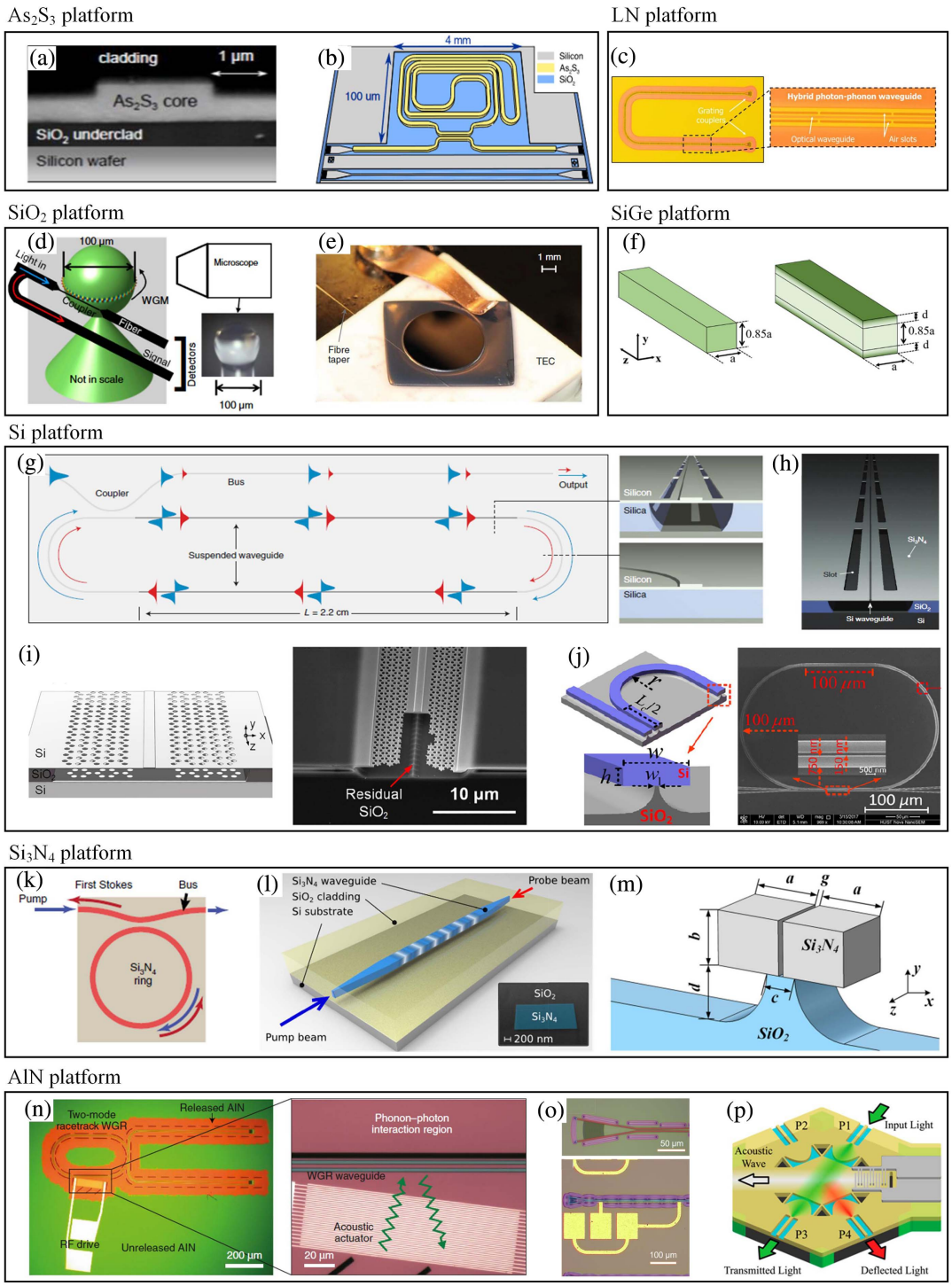

Fig. 4. Typical on-chip SBS devices with different materials and structures. (a) As_2S_3 rib waveguide on silica[16]; (b) As_2S_3 spiral ring resonator[25]; (c) suspended LN waveguide[91]; (d) SiO_2 microsphere[20]; (e) SiO_2 microdisk[23]; (f) SiGe alloy waveguide[46]; (g) suspended Si racetrack microring[53]; (h) suspended Si waveguide in Si_3N_4[26]; (i) Si waveguide with phononic crystals[3]; (j) Si waveguide with silica pillar[61]; (k) leaky Si_3N_4 microring[29]; (l) Si_3N_4 waveguide[70]; (m) Si_3N_4 slot waveguide[54]; (n) suspended AlN microring[30]; (o) suspended AlN waveguide[56]; (p) suspended AlN membrane[90].

predicted to exhibit high SBS gain in the mid-infrared band because it has lower acoustic velocity and a higher refractive index than silica[71]. However, its intrinsic loss in the communication band is relatively high (Table 1). This problem may be solved utilizing a SiGe alloy[46]. By optimizing the SiGe alloy composition, net Stokes amplification can achieve at least a 2.5 dB gain improvement compared to a pure Si waveguide. In addition, since the acoustic waves can be excited externally,

Table 1. Different Material Platforms and the Corresponding Properties for On-Chip SBS[a].

Material	Intrinsic Loss (dB/cm)	Refractive Index	Photoelastic Coefficient (p_{11}, p_{12})	Acoustic Velocity (m/s)	Density (kg/m^3)	Piezoelectric Coefficient (d_{13}, d_{33}) (pm/V)
As_2S_3	< 0.01	2.4	(+0.24, +0.25)	2527	3430	N/A
SiO_2	$< 1.4 \times 10^{-5}$	1.45	(+0.12, +0.27)	5915	2203	N/A
Si	< 0.01	3.5	(−0.09, +0.017)	8909	2330	N/A
Ge	< 3	4	(−0.151, −0.128)	5235	5350	N/A
Si_3N_4	< 0.004	2	(*, ±0.047)	10,500	3100	N/A
AlN	< 0.13	2.15	(−0.1, −0.027)	10,970	3257	(−2.65, 5.53)
LN	< 0.002	2.237	(−0.026, 0.07)	3491–4004	4628	(−4.64, −43.70)

[a]These data are taken from Refs. [2,29,63,64,70-75].

piezoelectric material is found to be a kind of outstanding material for external acoustic pumping. Brillouin acousto-optic interaction based on external acoustic injection is one of the most promising solutions for the future. Among piezoelectric materials, aluminium nitride (AlN) and lithium niobate (LN) are often used as an active material in Brillouin interactions and optomechanical interactions[30,31,56,57,83–91]. In general, the acoustic modes are electrically generated by interdigital transducers (IDTs) patterned on top of piezoelectric materials. With the design of a suspended structure, the good confinement of optical waves and the electrically induced acoustic waves greatly enhance Brillouin interactions and optomechanical interactions in active waveguides.

3.2. Applications of on-chip SBS

With the inherent narrow linewidth of SBS amplitude response, phase response, gigahertz frequency shift as well as group time delay[43,92], SBS-based devices have many particularly promising applications in microwave photonics (MWP) signal processing and optical communications, as shown in Fig. 5. Additionally, Fig. 6 displays the experimental setups and principles of partial on-chip SBS applications. The introduction of on-chip SBS can make these application platforms perform better in terms of high speed, high precision, and lightweight.

3.2.1. Microwave synthesizers

Since the microwave signal can be generated by the beat note between a pump wave and a Stokes wave, the Brillouin lasers mentioned above can provide promising solutions for microwave source synthesis with ultralow phase noise[41,93,94], and the linewidth of microwave source can be further narrowed if the Brillouin oscillators are in phonon lasing mode[29,95–97]. Additionally, optoelectronic oscillators (OEOs) based on SBS interactions can be used to generate microwave sources with low phase noise as well[34,98–100]. In the optoelectronic oscillators, the carrier signal undergoes a phase modulator seeded by white noise; then one of the side modes is amplified by an optical pump wave through SBS interactions in a Brillouin-active waveguide; finally, the beat note between the carrier signal and the amplified side mode is fed back into the phase modulator. Thus, the OEO begins oscillating above threshold and outputs microwave signals with low phase noise (< −100 dBc/Hz at 100 kHz offset frequency)[100]. Since the frequency of output microwave signals is determined by the frequency of the pump wave and the Brillouin shift, we can obtain widely tunable frequency of microwave signals (~40 GHz) by tuning the frequency of the pump wave.

3.2.2. MWP filters

MWP filters are one of the most important devices in microwave systems, which can be used to suppress interferences. Traditional optical filters such as Bragg gratings have relatively low resolution (~GHz)[101]. However, the narrow linewidth of SBS is quite suitable for narrowband MWP filters. The first MWP notch filter based on on-chip SBS was achieved in an As_2S_3 rib waveguide with a bandwidth of 126 MHz, a notch depth of 20 dB, and a frequency tunability in the range of 2–8 GHz[102]. Moreover, since the Brillouin gain is tailorable, the bandwidth of filter is also reconfigurable. A reconfigurable MWP filter was demonstrated with tunable bandwidth from 30 up to 440 MHz by electrically tailoring the pump, and the central frequency can be also continuously tunable up to 30 GHz while maintaining the frequency response[103]. Thereafter, MWP filters with an ultranarrow bandwidth of 3 MHz have been achieved based on Si waveguides as well[65,104].

3.2.3. Light storage and time-delay components

Light storage and time delay are critical to radar and signal synchronization[105]. According to the Kramers–Kronig relation, the SBS gain/loss spectra and the refractive index are uniquely correlated[106], which makes it possible to control the phase of microwave signals. Up to now, four different schemes of

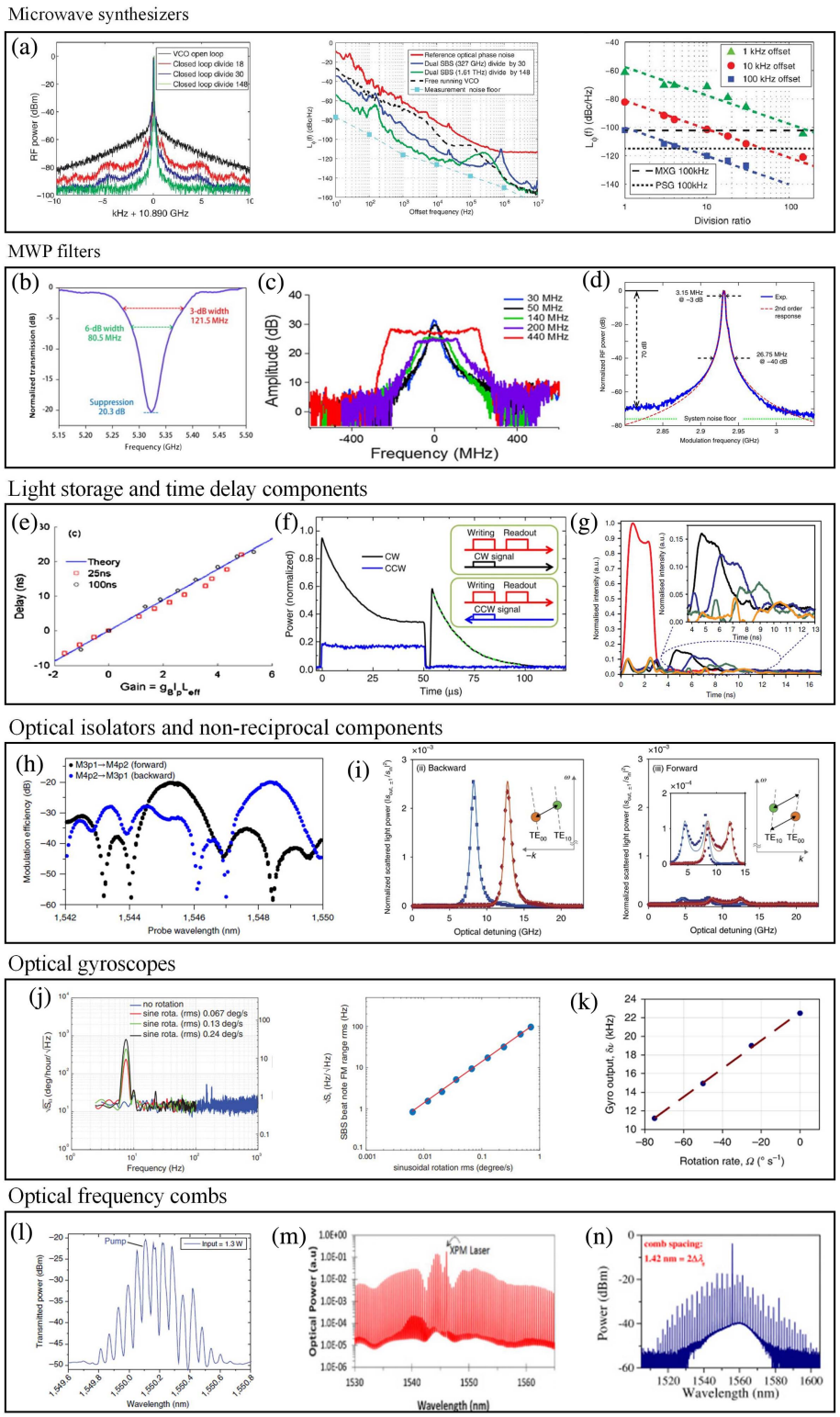

Fig. 5. Applications of on-chip SBS. (a) Microwave synthesizer based on SiO_2 microdisk[93]; (b) MWP filter based on As_2S_3 rib waveguide[102]; (c) reconfigurable MWP filter based on As_2S_3 rib waveguide[103]; (d) MWP filter based on Si waveguide[65]; (e) slow and fast light based on As_2S_3 rib waveguide[109]; (f) light storage based on SiO_2 microsphere[107]; (g) light storage based on As_2S_3 rib waveguide[32]; (h) isolator based on Si waveguide[55]; (i) isolator based on AlN microring with external acoustic pumping[30]; (j) optical gyroscope based on SiO_2 microdisk[39]; (k) optical gyroscope based on Si_3N_4 microring[29]; (l) optical frequency comb based on As_2S_3 rib waveguide[127]; (m) optical frequency comb based on As_2S_3 microring[128]; (n) optical frequency comb based on SiO_2 microbubble[129].

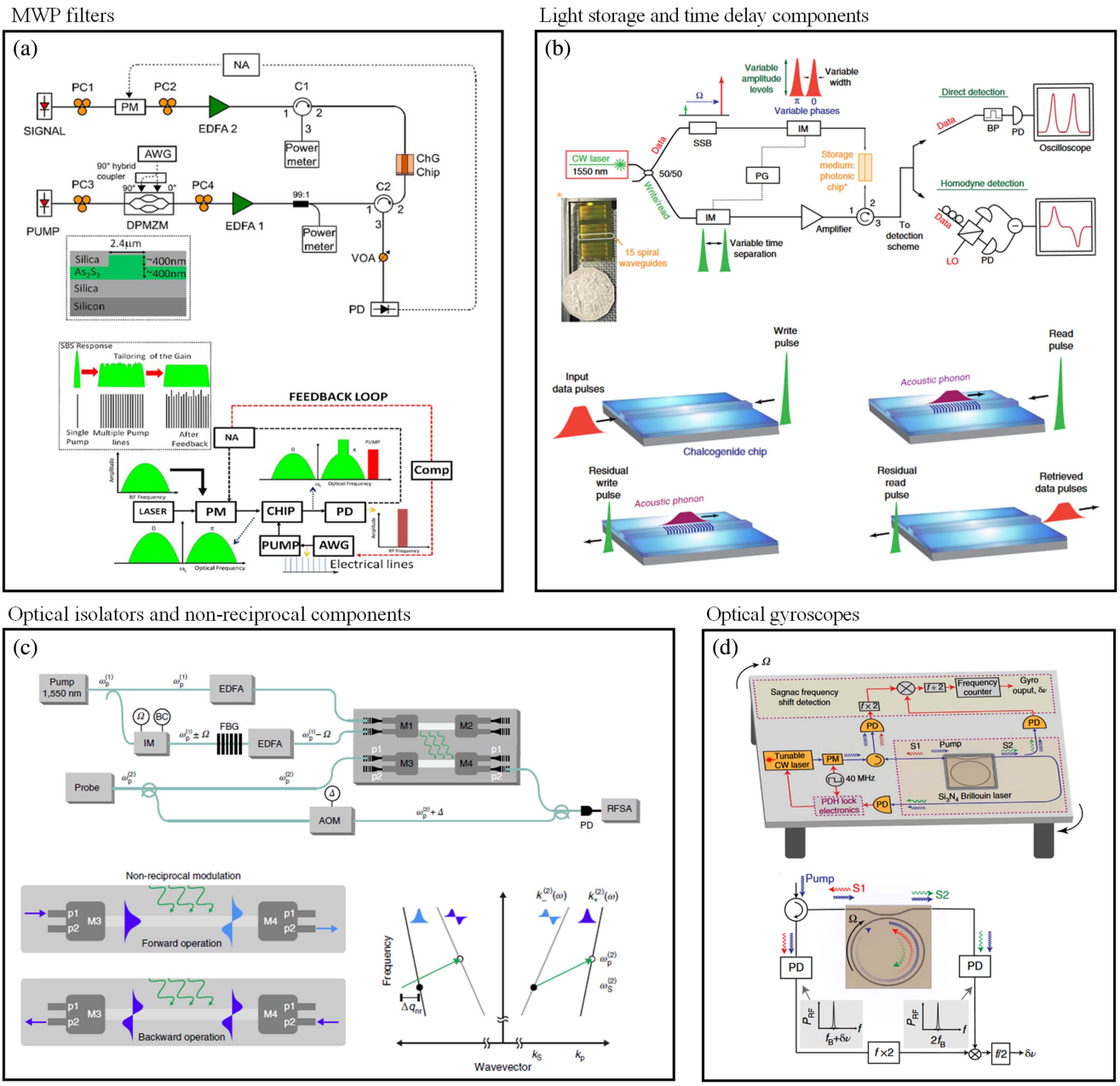

Fig. 6. Experimental setups and principles of on-chip SBS applications. (a) MWP filters[103]; (b) light storage and time-delay components[107]; (c) optical isolators and nonreciprocal components[55]; (d) optical gyroscopes[29].

time delay based on SBS have been demonstrated by slow light[107–109], dynamic gratings[110–112], quasi-light storage[113,114], and light storage[115,116]. Slow-light systems usually can be categorized in material slow-light and structural slow light[117]; slow light based on SBS belongs to the former. Compared to the electromagnetically induced transparency, which also belongs to material slow light, slow light based on SBS can work stably at room temperature. The first tunable slow and fast light based on on-chip SBS was demonstrated in an As_2S_3 rib waveguide with a maximum delay of ~23 ns[109], and the first light storage was demonstrated in a SiO_2 microsphere with a lifetime up to 10 μs[107], limited only by the phonon lifetime.

3.2.4. Optical isolators and nonreciprocal components

Nonreciprocal devices, in which the time-reversal symmetry of Maxwell's equations is broken for light propagation[30], can be applied as optical isolators and circulators. Although optical components such as waveguides, filters, couplers, lasers, modulators, and detectors have been already implemented in integrated photonics, it is still a big challenge to achieve on-chip nonreciprocal light propagation without magneto-optics, since the SBS process has unique phase-matching conditions, which depend on the direction of the pump wave. Hence, SBS is also a nonreciprocal process and can be utilized to achieve on-chip isolators and circulators. Nonreciprocal devices based on SBS

have the advantage of large bandwidth (>25 nm) and signal strength linearly related to pump power or radio-frequency power (isolation > 20 dB)[8,118], showing great application prospects. The first on-chip demonstration was realized by intermodal FSBS in a Si waveguide[55], which showed a 38 dB isolation between forward light and backward light with an operation bandwidth of more than 125 GHz. Then nonreciprocal propagation was also achieved in an AlN microring through external acoustic pumping[30], which demonstrated a mode conversion asymmetry of 15 dB and efficiency of 17% over a bandwidth exceeding 1 GHz. By contrast, the devices based on external acoustic injection have smaller sizes. Most recently, isolator with low loss (0.74 dB) and high nonreciprocal contrast (>10 dB) has also been achieved in Si waveguides with the help of piezoelectric AlN film[119].

3.2.5. Optical gyroscopes

Optical gyroscopes are widely employed in commercial and military systems. Traditional optical gyroscopes need a Sagnac interferometer based on fiber or free-space resonator to detect the rotation rates[120–122]. In order to miniaturize and compact the gyroscopes, backward Brillouin lasing in microresonators can be used to measure the rotation as a function of frequency shift[39] because the counterpropagating lasers will experience an opposite frequency shift due to the Sagnac effect. The on-chip Brillouin optical gyroscope was first demonstrated in a SiO_2 microdisk with sinusoidal rotation rates as low as 22 deg/h[39], which is 40 times more than that of previous experimental micro-optical systems. After that, gyroscope was also realized in a Si_3N_4 microring with an angle random walk of 8.52 deg/$h^{1/2}$ and bias instability of 58.7 deg/h[29,121], showing the great potential of on-chip high-precision Brillouin optical gyroscopes.

3.2.6. Optical frequency combs

Optical frequency combs play a quite important role in precision spectroscopy, atomic clocks, metrology, and chemical sensing[123–125]. The traditional optical frequency combs based on mode-locked lasers are limited by device size and cost. However, this status has gradually changed by the progress of compact, chip-scale microresonators. The cascading Brillouin lasing in ultrahigh Q microresonators enables the generation of highly coherent frequency combs with a gigahertz repetition rate[126]. The Brillouin frequency comb was first demonstrated in an As_2S_3 rib waveguide with 15 Brillouin lasing lines[127]. After that, a Brillouin frequency comb based on an As_2S_3 microring achieved wavelength across 1532.9–1557.5 nm and comb spacing of 40 GHz, which enables coherent optical communications using the advanced modulation format 64-QAM[128]. WGRs such as microbubble[129] also demonstrated high-performance frequency combs at communication wavelengths. When the double balance of nonlinearity and dispersion as well as dissipation and gain is satisfied, soliton frequency combs can then be observed[125,130].

4. Outlook and Conclusion

Brillouin interactions have attracted extensive attention owing to their unique acousto-optic properties. In this paper, we have reviewed and summarized the fundamental principle and diverse applications of on-chip SBS. With the maturity of integrated photonics and nanophotonics, multiple material platforms such as As_2S_3, SiO_2, Si/Si_3N_4, and various structures have been developed to implement efficient Brillouin acousto-optic interactions. The traditional Brillouin integrated photonics interacting with the optically excited acoustic waves are confronted with the problems of larger size and higher pump power[53]. In this condition, the piezoelectric materials such as AlN and LN with excellent properties have become popular, which demonstrate large acousto-optic coupling and electromechanical coupling efficiencies simultaneously. The electrically excited acoustic waves in piezoelectric materials greatly increase the Brillouin coupling strength and make the Brillouin devices more efficient and compact[31]. For the field of fundamental studies, Brillouin devices offer new opportunities for quantum technology[131–133]. Phonon squeezing, phonon cooling, and the strong coupling of Brillouin optomechanics are expected to achieve quantum state transfer, memory, and transduction. For the application aspect, Brillouin fiber sensing has been used to monitor crucial structures, since Brillouin frequency shifts exhibit sensitivity to environmental factors such as temperature and strain. In this context, on-chip Brillouin sensing becomes attractive. A recent experiment has shown the first demonstration of the submillimeter Brillouin optical correlation domain analysis measurement on a chip scale[134]. Since the phase conditions are sensitive to the resonant peak spacing of the microcavities, the on-chip Brillouin can be utilized to monitor the resonant drift and thermal information[135]. Furthermore, the current on-chip Brillouin devices are mostly independent and can be monolithically integrated on a single chip to achieve system-level applications in the future. In brief, we believe that on-chip SBS will continue to thrive and can be applied to many other fields with promising prospects.

Acknowledgements

This work was supported by the National Natural Science Foundation of China (Nos. 61875063 and 62175074).

References

1. L. Brillouin, "Diffusion de la lumière et des rayons X par un corps transparent homogène," Ann. Phys. **9**, 88 (1922).
2. B. J. Eggleton, C. G. Poulton, P. T. Rakich, *et al.*, "Brillouin integrated photonics," Nat. Photonics **13**, 664 (2019).
3. K. Wang, M. Cheng, H. Shi, *et al.*, "Demonstration of forward Brillouin gain in a hybrid photonic–phononic silicon waveguide," ACS Photonics **8**, 2755 (2021).
4. R. Y. Chiao, C. H. Townes, and B. P. Stoicheff, "Stimulated Brillouin scattering and coherent generation of intense hypersonic waves," Phys. Rev. Lett. **12**, 592 (1964).
5. E. P. Ippen and R. H. Stolen, "Stimulated Brillouin scattering in optical fibers," Appl. Phys. Lett. **21**, 539 (1972).

6. K. O. Hill, B. S. Kawasaki, and D. C. Johnson, "cw Brillouin laser," Appl. Phys. Lett. **28**, 608 (1976).
7. V. P. Kalosha, E. A. Ponomarev, L. Chen, *et al.*, "How to obtain high spectral resolution of SBS-based distributed sensing by using nanosecond pulses," Opt. Express **14**, 2071 (2006).
8. X. Huang and S. Fan, "Complete all-optical silica fiber isolator via stimulated Brillouin scattering," J. Light. Technol. **29**, 2267 (2011).
9. L. Thévenaz, "Slow and fast light in optical fibres," Nat. Photonics **2**, 474 (2008).
10. K. Y. Song and K. Hotate, "25 GHz bandwidth Brillouin slow light in optical fibers," Opt. Lett. **32**, 217 (2007).
11. J. M. C. Boggio, J. D. Marconi, and H. L. Fragnito, "Experimental and numerical investigation of the SBS-threshold increase in an optical fiber by applying strain distributions," J. Light. Technol. **23**, 3808 (2005).
12. R. G. Harrison, V. I. Kovalev, W. Lu, *et al.*, "SBS self-phase conjugation of CW Nd:YAG laser radiation in an optical fibre," Opt. Commun. **163**, 208 (1999).
13. A. Mocofanescu, X. Zhu, L. Wang, *et al.*, "Recent studies of CW stimulated Brillouin scattering (SBS) in single mode and multimode optical fibers," in *Conference on Lasers and Electro-Optics/Quantum Electronics and Laser Science and Photonic Applications Systems Technologies* (2005), paper CMCC6.
14. B. C. Rodgers, T. H. Russell, and W. B. Roh, "Laser beam combining and cleanup by stimulated Brillouin scattering in a multimode optical fiber," Opt. Lett. **24**, 1124 (1999).
15. P. Dainese, P. S. J. Russell, N. Joly, *et al.*, "Stimulated Brillouin scattering from multi-GHz-guided acoustic phonons in nanostructured photonic crystal fibres," Nat. Phys. **2**, 388 (2006).
16. R. Pant, C. G. Poulton, D.-Y. Choi, *et al.*, "On-chip stimulated Brillouin scattering," Opt. Express **19**, 8285 (2011).
17. P. T. Rakich, C. Reinke, R. Camacho, *et al.*, "Giant enhancement of stimulated Brillouin scattering in the subwavelength limit," Phys. Rev. X **2**, 011008 (2012).
18. P. T. Rakich, P. Davids, and Z. Wang, "Tailoring optical forces in waveguides through radiation pressure and electrostrictive forces," Opt. Express **18**, 14439 (2010).
19. W. Qiu, P. T. Rakich, H. Shin, *et al.*, "Stimulated Brillouin scattering in nanoscale silicon step-index waveguides: a general framework of selection rules and calculating SBS gain," Opt. Express **21**, 31402 (2013).
20. M. Tomes and T. Carmon, "Photonic micro-electromechanical systems vibrating at X-band (11-GHz) rates," Phys. Rev. Lett. **102**, 113601 (2009).
21. S. Zhu, B. Xiao, B. Jiang, *et al.*, "Tunable Brillouin and Raman microlasers using hybrid microbottle resonators," Nanophotonics **8**, 931 (2019).
22. G. Bahl, J. Zehnpfennig, M. Tomes, *et al.*, "Stimulated optomechanical excitation of surface acoustic waves in a microdevice," Nat. Commun. **2**, 403 (2011).
23. H. Lee, T. Chen, J. Li, *et al.*, "Chemically etched ultrahigh-*Q* wedge-resonator on a silicon chip," Nat. Photonics **6**, 369 (2012).
24. K. Y. Yang, D. Y. Oh, S. H. Lee, *et al.*, "Bridging ultrahigh-*Q* devices and photonic circuits," Nat. Photonics **12**, 297 (2018).
25. B. Morrison, A. Casas-Bedoya, G. Ren, *et al.*, "Compact Brillouin devices through hybrid integration on silicon," Optica **4**, 847 (2017).
26. H. Shin, W. Qiu, R. Jarecki, *et al.*, "Tailorable stimulated Brillouin scattering in nanoscale silicon waveguides," Nat. Commun. **4**, 1944 (2013).
27. R. Van Laer, B. Kuyken, D. Van Thourhout, *et al.*, "Interaction between light and highly confined hypersound in a silicon photonic nanowire," Nat. Photonics **9**, 199 (2015).
28. E. A. Kittlaus, N. T. Otterstrom, and P. T. Rakich, "On-chip inter-modal Brillouin scattering," Nat. Commun. **8**, 15819 (2017).
29. S. Gundavarapu, G. M. Brodnik, M. Puckett, *et al.*, "Sub-hertz fundamental linewidth photonic integrated Brillouin laser," Nat. Photonics **13**, 60 (2019).
30. D. B. Sohn, S. Kim, and G. Bahl, "Time-reversal symmetry breaking with acoustic pumping of nanophotonic circuits," Nat. Photonics **12**, 91 (2018).
31. Q. Liu, H. Li, and M. Li, "Electromechanical Brillouin scattering in integrated optomechanical waveguides," Optica **6**, 778 (2019).
32. M. Merklein, B. Stiller, K. Vu, *et al.*, "A chip-integrated coherent photonic-phononic memory," Nat. Commun. **8**, 574 (2017).
33. D. Marpaung, B. Morrison, M. Pagani, *et al.*, "Low-power, chip-based stimulated Brillouin scattering microwave photonic filter with ultrahigh selectivity," Optica **2**, 76 (2015).
34. R. Pant, D. Marpaung, I. V. Kabakova, *et al.*, "On-chip stimulated Brillouin Scattering for microwave signal processing and generation," Laser Photonics Rev. **8**, 653 (2014).
35. C. G. Poulton, R. Pant, A. Byrnes, *et al.*, "Design for broadband on-chip isolator using stimulated Brillouin scattering in dispersion-engineered chalcogenide waveguides," Opt. Express **20**, 21235 (2012).
36. A. Byrnes, R. Pant, E. Li, *et al.*, "Photonic chip based tunable and reconfigurable narrowband microwave photonic filter using stimulated Brillouin scattering," Opt. Express **20**, 18836 (2012).
37. J. Ma, J. Wen, S. Ding, *et al.*, "Chip-based optical isolator and nonreciprocal parity-time symmetry induced by stimulated Brillouin scattering," Laser Photonics Rev. **14**, 1900278 (2020).
38. Y.-H. Lai, M.-G. Suh, Y.-K. Lu, *et al.*, "Earth rotation measured by a chip-scale ring laser gyroscope," Nat. Photonics **14**, 345 (2020).
39. J. Li, M.-G. Suh, and K. Vahala, "Microresonator Brillouin gyroscope," Optica **4**, 346 (2017).
40. J. Li, H. Lee, T. Chen, *et al.*, "Characterization of a high coherence, Brillouin microcavity laser on silicon," Opt. Express **20**, 20170 (2012).
41. J. Li, H. Lee, and K. J. Vahala, "Microwave synthesizer using an on-chip Brillouin oscillator," Nat. Commun. **4**, 2097 (2013).
42. N. T. Otterstrom, E. A. Kittlaus, S. Gertler, *et al.*, "Resonantly enhanced nonreciprocal silicon Brillouin amplifier," Optica **6**, 1117 (2019).
43. B. J. Eggleton, C. G. Poulton, and R. Pant, "Inducing and harnessing stimulated Brillouin scattering in photonic integrated circuits," Adv. Opt. Photonics **5**, 536 (2013).
44. P. Kharel, R. O. Behunin, W. H. Renninger, *et al.*, "Noise and dynamics in forward Brillouin interactions," Phys. Rev. A **93**, 063806 (2016).
45. S. Gertler, P. Kharel, E. A. Kittlaus, *et al.*, "Shaping nonlinear optical response using nonlocal forward Brillouin interactions," New J. Phys. **22**, 043017 (2020).
46. M. Cheng, R. Zhang, K. Wang, *et al.*, "Analysis of forward stimulated brillouin scattering in nanoscale SiGe waveguides by tailoring optical forces," J. Light. Technol. **37**, 1143 (2019).
47. N. Dostart, S. Kim, and G. Bahl, "Giant gain enhancement in surface-confined resonant stimulated Brillouin scattering," Laser Photonics Rev. **9**, 689 (2015).
48. L. Yu, M. Cheng, K. Wang, *et al.*, "Analysis of giant forward Brillouin gain enhancement in double-disk microcavities by tailoring optical forces," Opt. Laser Technol. **141**, 107173 (2021).
49. C. Wolff, P. Gutsche, M. J. Steel, *et al.*, "Impact of nonlinear loss on stimulated Brillouin scattering," J. Opt. Soc. Am. B **32**, 1968 (2015).
50. G. S. Wiederhecker, P. Dainese, and T. P. Mayer Alegre, "Brillouin optomechanics in nanophotonic structures," APL Photonics **4**, 071101 (2019).
51. M. K. Schmidt, C. G. Poulton, G. Z. Mashanovich, *et al.*, "Suspended mid-infrared waveguides for stimulated Brillouin scattering," Opt. Express **27**, 4976 (2019).
52. J. E. Sipe and M. J. Steel, "A Hamiltonian treatment of stimulated Brillouin scattering in nanoscale integrated waveguides," New J. Phys. **18**, 045004 (2016).
53. N. T. Otterstrom, R. O. Behunin, E. A. Kittlaus, *et al.*, "A silicon Brillouin laser," Science **360**, 1113 (2018).
54. K. Wang, J. Sun, and M. Cheng, "Design of partially suspended silicon nitride slot waveguides for efficient forward stimulated Brillouin scattering," IEEE Photon. J. **12**, 4501211 (2020).
55. E. A. Kittlaus, N. T. Otterstrom, P. Kharel, *et al.*, "Non-reciprocal interband Brillouin modulation," Nat. Photonics **12**, 613 (2018).
56. H. Shi, C. Huang, L. Yu, *et al.*, "Intramodal acousto-optic scattering of opto-piezomechanical device on aluminum nitride," J. Light. Technol. **41**, 6348 (2023).
57. Y. Linfeng, C. Ming, W. Kang, *et al.*, "Enhanced forward stimulated Brillouin scattering in aluminum nitride slot waveguides with acoustic pumping," Proc. SPIE **11767**, 1176708 (2021).
58. M. Cheng, K. Wang, and J. Sun, "Demonstration of enhanced four-wave mixing by harnessing stimulated Brillouin scattering within a suspended cascaded microring resonator," Appl. Phys. Lett. **118**, 231104 (2021).
59. E. A. Kittlaus, H. Shin, and P. T. Rakich, "Large Brillouin amplification in silicon," Nat. Photonics **10**, 463 (2016).
60. S. Gertler, N. T. Otterstrom, M. Gehl, *et al.*, "Narrowband microwave-photonic notch filters using Brillouin-based signal transduction in silicon," Nat. Commun. **13**, 1947 (2022).

61. R. Zhang, J. Sun, G. Chen, *et al.*, "Demonstration of highly efficient forward stimulated Brillouin scattering in partly suspended silicon nanowire racetrack resonators," Appl. Phys. Lett. **111**, 031102 (2017).
62. A. Casas-Bedoya, B. Morrison, M. Pagani, *et al.*, "Tunable narrowband microwave photonic filter created by stimulated Brillouin scattering from a silicon nanowire," Opt. Lett. **40**, 4154 (2015).
63. P. Li, J.-Y. Ou, G. Z. Mashanovich, *et al.*, "Tailorable stimulated Brillouin scattering in a partially suspended aluminium nitride waveguide in the visible range," Opt. Express **30**, 27092 (2022).
64. W. Wang, Y. Yu, Y. Li, *et al.*, "Tailorable Brillouin light scattering in a lithium niobate waveguide," Appl. Sci. **11**, 8390 (2021).
65. H. Shin, J. A. Cox, R. Jarecki, *et al.*, "Control of coherent information via on-chip photonic–phononic emitter–receivers," Nat. Commun. **6**, 6427 (2015).
66. R. Dehghannasiri, A. A. Eftekhar, and A. Adibi, "Observation of stimulated Brillouin scattering in Si_3N_4 waveguides," in *IEEE Photonics Conference (IPC)* (2017), p. 135.
67. G. Chen, R. Zhang, and J. Sun, "On-chip optical mode conversion based on dynamic grating in photonic-phononic hybrid waveguide," Sci. Rep. **5**, 10346 (2015).
68. R. Zhang and J. Sun, "Design of silicon phoxonic crystal waveguides for slow light enhanced forward stimulated Brillouin scattering," J. Light. Technol. **35**, 2917 (2017).
69. R. Zhang, G. Chen, and J. Sun, "Analysis of acousto-optic interaction based on forward stimulated Brillouin scattering in hybrid phononic-photonic waveguides," Opt. Express **24**, 13051 (2016).
70. F. Gyger, J. Liu, F. Yang, *et al.*, "Observation of stimulated Brillouin scattering in silicon nitride integrated waveguides," Phys. Rev. Lett. **124**, 013902 (2020).
71. C. Wolff, R. Soref, C. G. Poulton, *et al.*, "Germanium as a material for stimulated Brillouin scattering in the mid-infrared," Opt. Express **22**, 30735 (2014).
72. Z. Luo, A. Zhang, W. Huang, *et al.*, "Aluminum nitride thin film based reconfigurable integrated photonic devices," IEEE J. Sel. Top. Quantum Electron. **29**, 9300119 (2023).
73. R. M. R. Pinto, V. Gund, R. A. Dias, *et al.*, "CMOS-integrated aluminum nitride MEMS: a review," J. Microelectromech. Syst. **31**, 500 (2022).
74. A. Shams-Ansari, G. Huang, L. He, *et al.*, "Reduced material loss in thin-film lithium niobate waveguides," APL Photonics **7**, 081301 (2022).
75. Y. Sun, W. Shin, D. A. Laleyan, *et al.*, "Ultrahigh *Q* microring resonators using a single-crystal aluminum-nitride-on-sapphire platform," Opt. Lett. **44**, 5679 (2019).
76. A. Choudhary, B. Morrison, I. Aryanfar, *et al.*, "Advanced integrated microwave signal processing with giant on-chip Brillouin gain," J. Light. Technol. **35**, 846 (2017).
77. I. Aryanfar, D. Marpaung, A. Choudhary, *et al.*, "Chip-based Brillouin radio frequency photonic phase shifter and wideband time delay," Opt. Lett. **42**, 1313 (2017).
78. D. K. Armani, T. J. Kippenberg, S. M. Spillane, *et al.*, "Ultra-high-*Q* toroid microcavity on a chip," Nature **421**, 925 (2003).
79. R. V. Laer, A. Bazin, B. Kuyken, *et al.*, "Net on-chip Brillouin gain based on suspended silicon nanowires," New J. Phys. **17**, 115005 (2015).
80. Y. Zhang, X. Xi, X. Sun, *et al.*, "Brillouin-active silicon nano-waveguide suspended on periodic pillars," in *TENCON 2022-2022 IEEE Region 10 Conference (TENCON)* (2022), p. 1.
81. K. Wang, M. Cheng, H. Shi, *et al.*, "Demonstration of stimulated Brillouin scattering in a silicon suspended microring with photonic-phononic waveguide," J. Light. Technol. **40**, 121 (2022).
82. R. Botter, K. Ye, Y. Klaver, *et al.*, "Guided-acoustic stimulated Brillouin scattering in silicon nitride photonic circuits," Sci. Adv. **8**, eabq2196 (2022).
83. M. Cheng, K. Wang, and J. Sun, "Efficient Brillouin optomechanical interaction assisted by piezomechanics on the SOI platform," IEEE Photon. J. **13**, 6600609 (2021).
84. Y. Zhou, F. Ruesink, S. Gertler, *et al.*, "Wideband nonmagnetic isolators in silicon photonics," in *Frontiers in Optics + Laser Science 2022 (FIO, LS)* (2022), paper FTu6C.3.
85. Y. Zhou, F. Ruesink, S. Gertler, *et al.*, "Intermodal strong coupling and wideband, low-loss isolation in silicon," in *CLEO 2023* (2023), paper SM4P.1.
86. E. A. Kittlaus, W. M. Jones, P. T. Rakich, *et al.*, "Electrically driven acousto-optics and broadband non-reciprocity in silicon photonics," Nat. Photonics **15**, 43 (2021).
87. D. B. Sohn, O. E. Örsel, and G. Bahl, "Electrically driven optical isolation through phonon-mediated photonic Autler–Townes splitting," Nat. Photonics **15**, 822 (2021).
88. L. Shao, M. Yu, S. Maity, *et al.*, "Microwave-to-optical conversion using lithium niobate thin-film acoustic resonators," Optica **6**, 1498 (2019).
89. C. C. Rodrigues, R. O. Zurita, T. P. M. Alegre, *et al.*, "Stimulated Brillouin scattering by surface acoustic waves in lithium niobate waveguides," J. Opt. Soc. Am. B **40**, D56 (2023).
90. H. Li, Q. Liu, and M. Li, "Electromechanical Brillouin scattering in integrated planar photonics," APL Photonics **4**, 080802 (2019).
91. O. E. Örsel and G. Bahl, "Piezoelectrically enhanced stimulated Brillouin scattering in $LiNbO_3$ thin films," in *Frontiers in Optics + Laser Science 2022 (FIO, LS)* (2022), paper FW7E.1.
92. M. Merklein, A. Casas-Bedoya, D. Marpaung, *et al.*, "Stimulated Brillouin scattering in photonic integrated circuits: novel applications and devices," IEEE J. Sel. Top. Quantum Electron. **22**, 336 (2016).
93. J. Li, X. Yi, H. Lee, *et al.*, "Electro-optical frequency division and stable microwave synthesis," Science **345**, 309 (2014).
94. R. Pant, E. Li, D. Y. Choi, *et al.*, "Cavity enhanced stimulated Brillouin scattering in an optical chip for multiorder Stokes generation," Opt. Lett. **36**, 3687 (2011).
95. R. Van Laer, R. Baets, and D. Van Thourhout, "Unifying Brillouin scattering and cavity optomechanics," Phys. Rev. A **93**, 053828 (2016).
96. J. Kim, M. C. Kuzyk, K. Han, *et al.*, "Non-reciprocal Brillouin scattering induced transparency," Nat. Phys. **11**, 275 (2015).
97. M.-G. Suh, Q.-F. Yang, and K. J. Vahala, "Phonon-limited-linewidth of Brillouin lasers at cryogenic temperatures," Phys. Rev. Lett. **119**, 143901 (2017).
98. Z. Zhu, M. Merklein, D.-Y. Choi, *et al.*, "Highly sensitive, broadband microwave frequency identification using a chip-based Brillouin optoelectronic oscillator," Opt. Express **27**, 12855 (2019).
99. M. Merklein, B. Stiller, I. V. Kabakova, *et al.*, "Opto-electronic oscillator employing photonic-chip based stimulated Brillouin scattering," in *Photonics and Fiber Technology* (2016), paper NW3A.6.
100. M. Merklein, B. Stiller, I. V. Kabakova, *et al.*, "Widely tunable, low phase noise microwave source based on a photonic chip," Opt. Lett. **41**, 4633 (2016).
101. D. Marpaung, J. Yao, and J. Capmany, "Integrated microwave photonics," Nat. Photonics **13**, 80 (2019).
102. B. Morrison, D. Marpaung, R. Pant, *et al.*, "Tunable microwave photonic notch filter using on-chip stimulated Brillouin scattering," Opt. Commun. **313**, 85 (2014).
103. A. Choudhary, I. Aryanfar, S. Shahnia, *et al.*, "Tailoring of the Brillouin gain for on-chip widely tunable and reconfigurable broadband microwave photonic filters," Opt. Lett. **41**, 436 (2016).
104. S. Gertler, E. A. Kittlaus, N. T. Otterstrom, *et al.*, "Microwave filtering using forward Brillouin scattering in photonic-phononic emit-receive devices," J. Light. Technol. **38**, 5248 (2020).
105. M. Merklein, B. Stiller, and B. J. Eggleton, "Brillouin-based light storage and delay techniques," J. Opt. **20**, 083003 (2018).
106. J. T. Mok and B. J. Eggleton, "Expect more delays," Nature **433**, 811 (2005).
107. C.-H. Dong, Z. Shen, C.-L. Zou, *et al.*, "Brillouin-scattering-induced transparency and non-reciprocal light storage," Nat. Commun. **6**, 6193 (2015).
108. L. McKay, M. Merklein, A. C. Bedoya, *et al.*, "Brillouin-based phase shifter in a silicon waveguide," Optica **6**, 907 (2019).
109. R. Pant, A. Byrnes, C. G. Poulton, *et al.*, "Photonic-chip-based tunable slow and fast light via stimulated Brillouin scattering," Opt. Lett. **37**, 969 (2012).
110. Y. Antman, N. Levanon, and A. Zadok, "Low-noise delays from dynamic Brillouin gratings based on perfect Golomb coding of pump waves," Opt. Lett. **37**, 5259 (2012).
111. H. Zhang and Y. Dong, "Advances in Brillouin dynamic grating in optical fibers and its applications," Prog. Quantum Electron. **87**, 100440 (2023).
112. M. Santagiustina, S. Chin, N. Primerov, *et al.*, "All-optical signal processing using dynamic Brillouin gratings," Sci. Rep. **3**, 1594 (2013).
113. S. Preussler, A. Wiatrek, K. Jamshidi, *et al.*, "Quasi-light-storage enhancement by reducing the Brillouin gain bandwidth," Appl. Opt. **50**, 4252 (2011).
114. S. Preußler, K. Jamshidi, A. Wiatrek, *et al.*, "Quasi-Light-Storage based on time-frequency coherence," Opt. Express **17**, 15790 (2009).

115. Z. Zhu, D. J. Gauthier, and R. W. Boyd, "Stored light in an optical fiber via stimulated brillouin scattering," Science **318**, 1748 (2007).
116. V. P. Kalosha, W. Li, F. Wang, *et al.*, "Frequency-shifted light storage via stimulated Brillouin scattering in optical fibers," Opt. Lett. **33**, 2848 (2008).
117. R. W. Boyd, "Material slow light and structural slow light: similarities and differences for nonlinear optics [Invited]," J. Opt. Soc. Am. B **28**, A38 (2011).
118. C. G. Poulton, R. Pant, A. Byrnes, *et al.*, "Design for broadband on-chip isolator using stimulated Brillouin scattering in dispersion-engineered chalcogenide waveguides," Opt. Express **20**, 21235 (2012).
119. Y. Zhou, F. Ruesink, S. Gertler, *et al.*, "Intermodal strong coupling and wideband, low-loss isolation in silicon," arXiv:2211.05864 (2022).
120. B. Wu, Y. Yu, J. Xiong, *et al.*, "Silicon integrated interferometric optical gyroscope," Sci. Rep. **8**, 8766 (2018).
121. S. Gundavarapu, M. Belt, T. A. Huffman, *et al.*, "Interferometric optical gyroscope based on an integrated Si_3N_4 low-loss waveguide coil," J. Light. Technol. **36**, 1185 (2018).
122. H. C. Lefèvre, "The fiber-optic gyroscope: challenges to become the ultimate rotation-sensing technology," Opt. Fiber Technol. **19**, 828 (2013).
123. T. J. Kippenberg, R. Holzwarth, and S. A. Diddams, "Microresonator-based optical frequency combs," Science **332**, 555 (2011).
124. A. L. Gaeta, M. Lipson, and T. J. Kippenberg, "Photonic-chip-based frequency combs," Nat. Photonics **13**, 158 (2019).
125. T. J. Kippenberg, A. L. Gaeta, M. Lipson, *et al.*, "Dissipative Kerr solitons in optical microresonators," Science **361**, eaan8083 (2018).
126. D. Braje, L. Hollberg, and S. Diddams, "Brillouin-enhanced hyperparametric generation of an optical frequency comb in a monolithic highly nonlinear fiber cavity pumped by a cw laser," Phys. Rev. Lett. **102**, 193902 (2009).
127. M. Merklein, I. V. Kabakova, T. F. S. Büttner, *et al.*, "Enhancing and inhibiting stimulated Brillouin scattering in photonic integrated circuits," Nat. Commun. **6**, 6396 (2015).
128. A. Choudhary, M. Pelusi, D. Marpaung, *et al.*, "On-chip Brillouin purification for frequency comb-based coherent optical communications," Opt. Lett. **42**, 5074 (2017).
129. Q. Lu, S. Liu, X. Wu, *et al.*, "Stimulated Brillouin laser and frequency comb generation in high-*Q* microbubble resonators," Opt. Lett. **41**, 1736 (2016).
130. Y. Bai, M. Zhang, Q. Shi, *et al.*, "Brillouin-Kerr soliton frequency combs in an optical microresonator," Phys. Rev. Lett. **126**, 063901 (2021).
131. A. D. Kashkanova, A. B. Shkarin, C. D. Brown, *et al.*, "Superfluid Brillouin optomechanics," Nat. Phys. **13**, 74 (2017).
132. G. Enzian, M. Szczykulska, J. Silver, *et al.*, "Observation of Brillouin optomechanical strong coupling with an 11 GHz mechanical mode," Optica **6**, 7 (2019).
133. H. Doeleman, T. Schatteburg, R. Benevides, *et al.*, "Brillouin optomechanics in the quantum ground state," arXiv:2303.04677 (2023).
134. A. Zarifi, B. Stiller, M. Merklein, *et al.*, "On-chip correlation-based Brillouin sensing: design, experiment, and simulation," J. Opt. Soc. Am. B **36**, 146 (2019).
135. J. Wang, R. Zhou, D. Lai, *et al.*, "Tuning on optical resonances of microcavities based on thermal dissipation control," IEEE Photon. Technol. Lett. **31**, 1175 (2019).